Clays and Clay Minerals, Vol. 59, No. 5, 466–477, 2011.

SYNTHESIS, CHARACTERIZATION, AND VISIBLE-LIGHT PHOTO-FENTON CATALYTIC ACTIVITY OF HYDROXY Fe/Al-INTERCALATED MONTMORILLONITE

HAILING LI[1], PINGXIAO WU[1,2,3,*], ZHI DANG[1,2,3], NENGWU ZHU[1,2,3], PING LI[1,2], AND JINHUA WU[1,2]

[1] College of Environmental Science and Engineering, South China University of Technology, Guangzhou 510006, P.R. China
[2] The Key Lab of Pollution Control and Ecosystem Restoration in Industry Clusters, Ministry of Education, Guangzhou 510006, P.R. China
[3] The Key Laboratory of Environmental Protection and Eco-Remediation of Guangdong Regular Higher Education Institutions, Guangzhou 510006, P.R. China

Abstract—The photochemically assisted Fenton reaction (photo-Fenton) is important because it may be particularly effective for the degradation of harmful organic compounds in the environment using solar light. The purpose of the present study was to determine the effectiveness of hydroxy Fe/Al-intercalated montmorillonites (Fe/Al-Mt) as photo-Fenton catalysts. In particular, different Fe/Al molar ratios were of interest as a means to vary catalytic activity. Intercalation was achieved *via* an ion-exchange method and brilliant orange X-GN was the test compound for photodegradation by hydrogen peroxide (H_2O_2) under visible-light irradiation ($\lambda > 420$ nm) in the presence of Fe/Al-Mt. The Fe/Al-Mt materials obtained were characterized by powder X-ray diffraction, N_2 adsorption/desorption, X-ray fluorescence spectroscopy, X-ray photoelectron spectroscopic analysis, and ultraviolet-visible spectroscopy. The decoloration performance of Fe/Al-Mt was investigated using different experimental parameters, including the synthesis method, the Fe/Al molar ratio of the intercalating solution, the catalyst dosage, the H_2O_2 dosage, and the pH. The results of photo-Fenton reaction showed that the photocatalytic activity of Fe/Al-Mt was enhanced significantly by the extent of hydroxy Al/Fe intercalation. For optimal reaction conditions, 99.92% degradation efficiency of X-GN was achieved after 140 min of reaction. To obtain further information on the visible-light-assisted photo-Fenton process, a high-performance liquid chromatography-mass spectrometry method was applied to indentify the intermediate products and a degradation pathway was proposed.

Key Words—Hydroxy Fe/Al, Photo-Fenton, Intercalated Montmorillonite, Visible Light.

INTRODUCTION

The tremendous range of synthetic dyes available today permits their extensive use in a number of industries such as textile, tannery, paint, plastics, and paper. However, dye-containing effluent discharged from these industries has become a major environmental issue. Up to 10−15% of the dyes used is released into the environment (Selvam *et al.*, 2003) with a resulting harmful effect on the environment and on human health due to the low biodegradability and toxic effect on living organisms of the dyes. Among various dyes available for textile processing, those used most commonly are azo dyes (van der Zee and Villaverde, 2005). In the present work, reactive brilliant orange (X-GN), a type of azo dye commonly used in China, which contains triazine as the reactive group, was selected as a model commercial dye.

Among the techniques available, advanced oxidation processes (AOPs) show significant promise for the efficient treatment of different kinds of refractory dyestuffs. An heterogeneous photo-Fenton process, which is an emerging AOP, has attracted considerable interest due to its excellent performance in the decomposition of various pollutants. Thus far, many kinds of solids have been proposed as catalysts or supports for catalysts; among them, clays have become an attractive alternative due to their accessibility and low cost (Dogan *et al*., 2007; Carriazo *et al*., 2010; Ramirez *et al*., 2011). The exchangeable cation located between the layers of these layered silicate minerals can be replaced by a variety of cations. Modification using different kinds of cations results in modification of the properties such as basal spacing, porosity, surface area, and surface acidity, which could facilitate the adsorption performance as well as catalytic features of the clays (Booij *et al*., 1996; Moreno *et al*., 1999; Aouad *et al.*, 2010). Previous studies have shown that many kinds of clays modified by polyhydroxy metals such as Al, Fe, or mixed complexes are effective at oxidation of organic compounds in water (Carriazo *et al*., 2008; Zuo *et al*., 2009; Caudo *et al*., 2007). Recently, clays modified by the Fe/Al copolymer have been studied extensively and are reported to show potential application in the fields of adsorbents (Jiang *et*

* E-mail address of corresponding author:
pppxwu@scut.edu.cn
DOI: 10.1346/CCMN.2011.0590504

https://doi.org/10.1346/CCMN.2011.0590504 Published online by Cambridge University Press

al., 2002) and catalysts that are active in the oxidation of organisms (Ladavos *et al*., 1996; Guélou *et al.*, 2003). Fe/Al pillared clays can avoid the leaching of dissolved Fe species (Barrault *et al*., 2000; Sanabria *et al.*, 2009), are less sensitive to pH (Catrinescu *et al*., 2003), and simultaneously favor the generation of OH· radicals (Molina *et al*., 2006).

The photo-Fenton reaction in an ultraviolet (UV)/H_2O_2 system has been reported extensively and proven to be efficient at dye degradation. Use of artificial UV light is a disadvantage and the research focus now is on utilizing solar energy and exploiting effective photocatalysts that are highly sensitive to visible light (sunlight) rather than UV light. According to the recent literature, little research has been done on the application of hydroxy Fe/Al clay as an heterogenous Fenton catalyst under visible light. In the present study, hydroxy Fe/Al-intercalated montmorillonite (Fe/Al-Mt) was prepared at different molar ratios of Fe/Al and its photo-Fenton catalytic properties were assessed under visible-light irradiation. Furthermore, degradation products were identified to reveal details of the visible-light-assisted photo-Fenton process.

MATERIALS AND METHODS

Materials

The calcium montmorillonite used here was obtained from Nanhai, Guangdong Province, P.R. China, and was purified and fractionated by the sedimentation method.

Reactive brilliant orange X-GN was purchased from Advanced Technology Industry, Ltd. (Hong Kong, P.R. China). $AlCl_3.6H_2O$, $FeCl_3.6H_2O$, Na_2CO_3, H_2O_2 (30%), NaOH, and HCl were of analytical grade and purchased from Guangzhou Chemical Reagent Factory (Guangzhou, P.R. China).

Synthesis of the catalysts

The hydroxy Fe/Al-intercalated montmorillonite was synthesized by intercalating the montmorillonite *via* cation exchange; the synthesis procedure was carried out as follows. A polymeric Al solution was prepared according to the method proposed by Zhu *et al.* (2009) but with some modification: 1 M Na_2CO_3 was added dropwise to a 0.5 M $AlCl_3$ solution under magnetic stirring; the temperature was kept at ~80ºC and the molar ratio of $[OH^-]/[Al^{3+}]$ was 2.4. A polymeric Fe solution was obtained by adding Na_2CO_3 powder slowly to a 0.2 M $FeCl_3$ solution under vigorous stirring until the molar ratio of $[Na_2CO_3]/[Fe^{3+}]$ was 0.75:1 (Chen *et al.*, 2009). Both the polymeric Al and Fe solutions were aged for 24 h at room temperature. The intercalating solution was prepared by adding the polymeric Fe solution slowly to the polymeric Al solution according to different Fe/Al molar ratios. After aging for 24 h at room temperature, the intercalating solution was added to 2 wt.% montmorillonite suspension at an [Al+Fe]/clay ratio of 10 mol/kg. In order to improve the dispersion of montmorillonite in water, the suspension was placed in an ultrasonic bath for 30 min. The resulting suspension was stirred for a further 3−4 h and then aged for 48 h at room temperature. The Fe/Al-Mt products were separated by filtration and then filter washed several times with distilled water. The samples were dried at 80ºC overnight and ground to a particle size which would pass through a 200 mesh sieve. The samples obtained with an Fe/Al molar ratio of 0.1, 0.3, 0.5, 0.8, 1.0, and 1.2 are denoted below as $FeAl_{0.1}$-Mt, $FeAl_{0.3}$-Mt, $FeAl_{0.5}$-Mt, $FeAl_{0.8}$-Mt, $FeAl_{1.0}$-Mt, and $FeAl_{1.2}$-Mt, respectively.

For a comparative study of the effect of synthesis method on the photocatalytic properties of the intercalated clay, another series of Fe/Al-Mt was synthesized adopting a similar procedure, except that the aging process for suspensions containing montmorillonite and Fe/Al intercalating solution was carried out at a temperature of 60ºC controlled by a water bath. The samples of this latter series are denoted hereafter as $FeAl_{0.2}$-Mt[a], $FeAl_{0.5}$-Mt[a], $FeAl_{0.8}$-Mt[a], $FeAl_{1.0}$-Mt[a], and $FeAl_{1.2}$-Mt[a].

Characterization methods

The X-ray diffraction (XRD) patterns of samples were obtained using a Rigaku D/MAX-IIIA X-ray diffractometer (Tokyo, Japan) with CuKα radiation over the 2θ range of ~3−70º.

Fourier-transform infrared (FTIR) spectra were recorded by the KBr pellet (KBr/sample mass ratio ~100/1) technique using a PerkinElmer 1725X FTIR spectrophotometer (Foster City, California, USA).

The chemical compositions of the samples were determined using a PANalytical PW-4400 X-ray fluorescence spectrometer (XRF) (Amsterdam, The Netherlands).

The surface areas of the materials were determined by adsorption of nitrogen at 77 K on a Micromeritics ASAP 2020 surface area and porosity analyzer (Atlanta, Georgia, USA).

X-ray photoelectron spectroscopy (XPS) measurements were carried out using an ANELVA AES-430S X-ray photoelectron spectrometer (Tokyo, Japan), with AlKα radiation as the excitation source and a constant pass energy of 40 eV, the binding energy (BE) of C 1s was corrected to 284.6 eV as an internal reference.

Ultraviolet-visible (UV-vis) diffuse-reflectance spectra were obtained using a Shimadzu 2501 PC UV-vis spectrophotometer (Kyoto, Japan). The reference material was $BaSO_4$.

Evaluation of catalytic activity

The photocatalytic performance of the Fe/Al-Mt was evaluated by the degradation of X-GN. The experiments were carried out in a 500 mL vessel which was placed in a water bath (with circulating water) to maintain the temperature at ~30±0.5ºC. A Philips 300 W halogen

https://doi.org/10.1346/CCMN.2011.0590504 Published online by Cambridge University Press

lamp was used as a source of visible light, using a cutoff filter to eliminate light of wavelengths of <420 nm.

Degradation of X-GN was conducted according to the following procedure: the pH of 200 mL of solution containing the desired X-GN concentration was adjusted using HCl and NaOH. Then a given amount of catalyst was added to the solution and the suspension was stirred in the dark for 15 min to allow the establishment of adsorption equilibrium. The photo-Fenton reaction was started with the halogen lamp turned on and the desired amount of H_2O_2 was added to the X-GN solution. At given intervals of decomposition, 2 mL samples were taken for analysis and each sample was filtered through a 0.45 μm filter membrane in the absence of visible light. The degradation of X-GN was analyzed using a 2450 UV-vis spectrophotometer (Shimadzu, Kyoto, Japan) at a wavelength of 479 nm, the maximum absorption wavelength of X-GN. The Fe ions leaching from the catalyst as a function of time were measured using a Zeeman 2000 atomic absorption spectrophotometer (Hitachi, Tokyo, Japan). Al ions leached also but were not measured.

Chromatographic and mass spectrometry conditions

The intermediates formed during the photo-Fenton reaction were identified by means of high-performance liquid chromatography-mass spectrometry (HPLC-MS) using an Esquire HCT PLUS Ion Trap Electro-Spray Mass Spectromet from Bruker (Germany). During the photo-Fenton process, samples were extracted from the reactor and filtered in the absence of visible light (as mentioned above), and then treated with 1 N NaOH to halt oxidation reaction prior to analysis (Kavitha and Palanivelu, 2004). The stationary phase was a C18 Luna column (150 mm × 2.00 mm, 5 μm, Phenomenex, USA). The mobile phase was an aqueous solution of acetonitrile, which was increased from 25% to 95% (acetonitrile/water, v/v) within 30 min and then kept for 10 min, at a flow rate of 0.2 mL/min. The injection volume was 5 μL. The mass spectrometer was operated in negative ion full-scan mode and in MS/MS mode, using an electron spray ion (ESI) source.

RESULTS AND DISCUSSION

Catalyst characterization

The chemical compositions (Table 1) reveal that the Al_2O_3 content in modified clays decreased, as expected, with increasing Fe/Al molar ratio. The Fe_2O_3 concentration reached a maximum at Fe/Al = 0.8, however, and then decreased slightly as the molar ratios reached 1.0 and 1.2. In intercalating solutions with smaller Fe/Al ratios, Fe probably coexisted with the Keggin polycation, and would have contributed to the collapse of the Keggin polycation with increasing Fe content. The latter might have led to separate hydrolysis of Fe and Al and competitive intercalation of Fe and Al into montmorillonite; thus the Fe content was decreased to a small degree.

After intercalation, the signal for the 001 peak at ~1.54 nm shifted to higher values of between 1.58 nm and 1.93 nm (Table 1), indicating that hydroxy Fe/Al groups intercalated the montmorillonite successfully. The 001 peak was broadened and its intensity weakened by the incorporation of Fe/Al complexes (Figure 1), indicating that the Fe/Al complexes were intercalated randomly into the interlayers of montmorillonite (Cristofara and Violante, 2001). The d_{001} values were clearly much greater at a relatively small Fe/Al molar ratio, while they decreased to 1.58 nm and 1.61 nm at Fe/Al = 1.0 and 1.2, respectively, similar to previous results in which an increase of the Fe content produced materials with little increase in the basal spacing (Caudo *et al.*, 2007; Letaef *et al.*, 2003; Luo *et al.*, 2009).

The d_{001} values of FeAl-Mt[a] ranged from 1.61 to 1.94 nm (Table 2), implying that the higher temperature (60ºC) had no significant effect on the basal spacing (Table 2). The increasing aging temperature does seem to have weakened the negative impact of excessive Fe loading on the basal spacing of the intercalated catalyst, as d_{001} values did not decrease as sharply as those of samples synthesized at room temperature. The intercalation of hydroxy Fe/Al groups yielded intercalated samples with greater specific surface areas of between 128 and 259 m^2/g compared to the starting

Table 1. Characterization of montmorillonite and Fe/Al-Mt by chemical analysis (wt.%), XRD, and surface area.

Samples	d_{001} (nm)	S_{BET}, surface area (m^2/g)	SiO_2	Al_2O_3	Fe_2O_3	MgO	CaO	Na_2O
Mt	1.54	76	73.57	12.07	2.00	4.06	2.016	0.37
$FeAl_{0.1}$-Mt	1.93	244	61.54	17.49	4.02	3.34	0.04	0.52
$FeAl_{0.3}$-Mt	1.84	210	61.87	17.28	4.81	3.38	0.046	0.53
$FeAl_{0.5}$-Mt	1.93	259	58.61	16.53	6.76	3.19	0.035	0.50
$FeAl_{0.8}$-Mt	1.89	234	61.63	15.48	8.13	3.15	0.033	0.53
$FeAl_{1.0}$-Mt	1.58	171	64.48	14.89	7.36	3.33	0.041	0.50
$FeAl_{1.2}$-Mt	1.61	128	64.52	13.86	7.96	3.31	0.043	0.54

$FeAl_x$-Mt with molar ratio of Fe/Al = x

https://doi.org/10.1346/CCMN.2011.0590504 Published online by Cambridge University Press

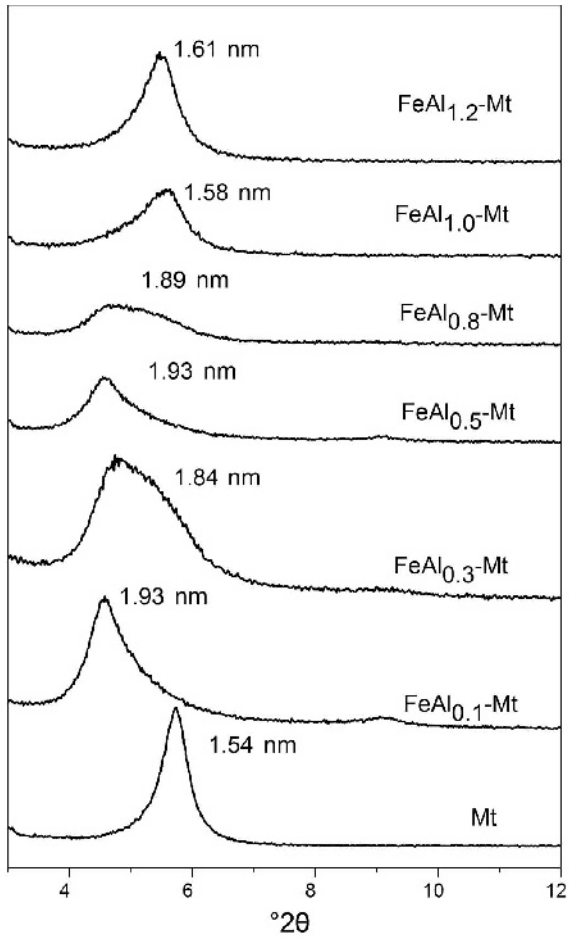

Figure 1. XRD patterns of montmorillonite and Fe/Al-Mt.

montmorillonite (76 m^2/g) (Table 1). In addition, the negative effect on the textural properties of Fe/Al-Mt induced by excessive Fe content was also observed in terms of the specific surface area, S_{BET}, (Table 1) where intercalation of the montmorillonite with Fe/Al molar ratios >0.8 gave smaller specific surface areas. The XRD results show that an intercalating agent with smaller Fe/Al ratio can prop the superimposed layers apart significantly, which facilitates the accessibility of the pores by N_2 and thus gives greater specific surface area, while increasing the Fe content is ineffective.

Table 2. d_{001} values for montmorillonite and Fe/Al-Mt synthesized at a different temperature.

Samples	d_{001} (nm)	Samples	d_{001} (nm)
Mt	1.54	$FeAl_{1.2}$-Mt	1.61
$FeAl_{0.1}$-Mt	1.93	$FeAl_{0.2}$-Mt[a]	1.81
$FeAl_{0.3}$-Mt	1.84	$FeAl_{0.5}$-Mt[a]	1.94
$FeAl_{0.5}$-Mt	1.93	$FeAl_{0.8}$-Mt[a]	1.71
$FeAl_{0.8}$-Mt	1.89	$FeAl_{1.0}$-Mt[a]	1.69
$FeAl_{1.0}$-Mt	1.58	$FeAl_{1.2}$-Mt[a]	1.61

[a] Fe/Al-Mt synthesized at 60ºC.

The FTIR spectra of Fe/Al-Mt show that several bands typical of montmorillonite (*i.e.* 3624 cm^{-1} for O–H stretching of structural O–H groups, 1087 cm^{-1} for Si–O stretching, 914 cm^{-1} of Al–Al–OH deformation, 795 cm for Si–O stretching of cristobalite, 626 cm^{-1} for coupled Al–O and Si–O out-of-plane stretching vibration, 519 cm^{-1} Al–O–Si deformation, and 467 cm^{-1} of Si–O–Si deformation) are nearly the same or the change in these bands is negligible after modification (Figure 2). Major change was observed in three areas of wavelength range, at ~3430 cm^{-1}, ~1640 cm^{-1}, and ~730 cm^{-1}. The absorption at ~3430 cm^{-1} can be assigned to the symmetric O–H stretching vibration of H-bonded water (Madejová *et al.*, 2002); the frequency shifted to a higher, then back to a lower, wavenumber with increasing Fe/Al molar ratio. Comparison between intercalated samples revealed that Fe contributed to the decrease of hydrogen-bonding strength in Fe/Al-Mt. Meanwhile, the H–O–H bending vibration at 1642 cm^{-1} found in montmorillonite shifted to 1637 or 1638 cm^{-1} after intercalation.

To further study the chemical and structural change in montmorillonite by the intercalation process, XPS analysis was carried out and high-resolution spectra of the Fe 2p electron binding energies were recorded. The main peak for montmorillonite due to the original structural Fe species located in montmorillonite was

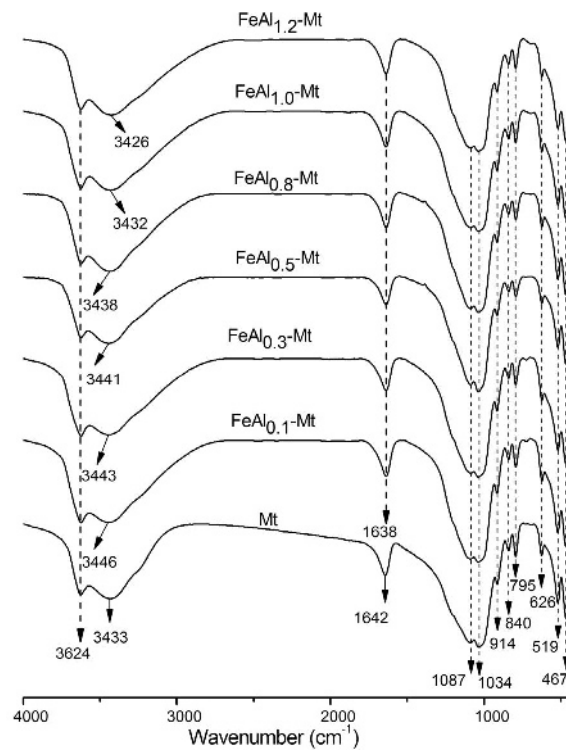

Figure 2. FTIR spectra of montmorillonite and Fe/Al-Mt.

https://doi.org/10.1346/CCMN.2011.0590504 Published online by Cambridge University Press

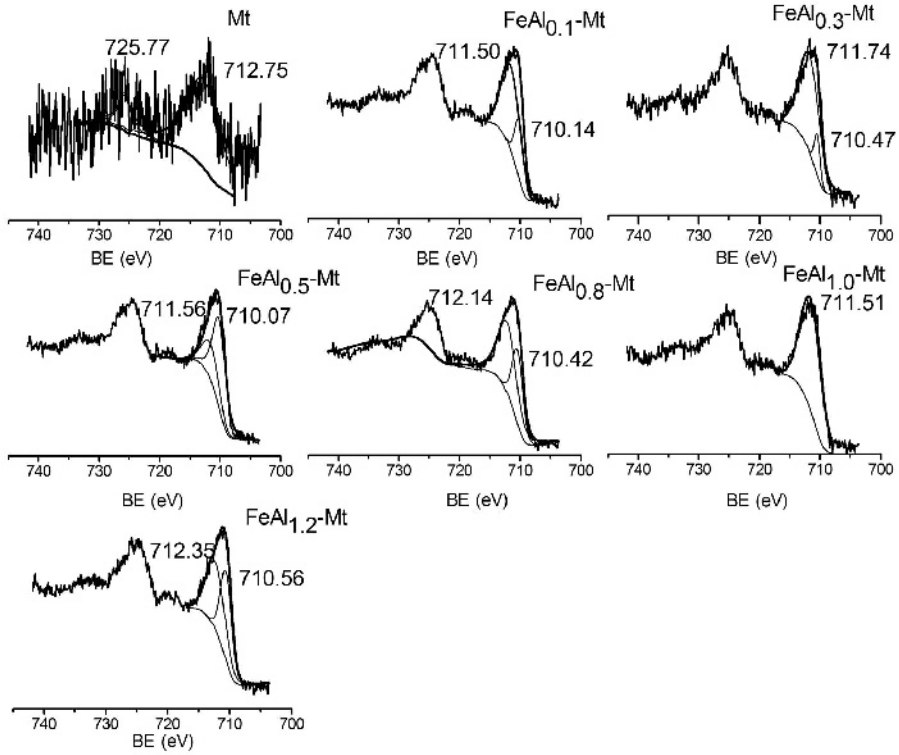

Figure 3. High-resolution XPS analysis for Fe 2p (BE = binding energy) in montmorillonite and Fe/Al-Mt.

present at 712.75 eV (Figure 3). Intercalation of Fe/Al complexes brought new peaks for Fe, positioned at ~710 eV (assigned to Fe oxide), ~711 eV, and 712 eV (the latter two assigned to Fe hydroxide).

Compared with montmorillonite, the UV-vis spectra of Fe/Al-Mt showed a significant absorption shift to the visible region (Figure 4). The adsorption edge of montmorillonite was observed at ~350 nm and expanded to ~590 nm after intercalation, making possible the use of visible light by the intercalated catalyst. The starting montmorillonite displayed a band centered at 247 nm, arising from the presence of structural Fe(III) species (Fe(III)O) either tetrahedrally or octahedrally coordinated in the montmorillonite framework (Rao *et al.*, 2005; Chmielarz *et al.*, 2007; Fejes *et al.*, 2002; Ali *et al.*, 2009). When the Fe content of the samples increased, a broad band appeared with comparable absorption intensity at ~350 nm, with this band assigned to FeO_x species (Bachari *et al.*, 2007; Chmielarz *et al.*, 2007) or oligomeric clusters (Schwidder *et al.*, 2005). The shoulder band at 481 nm appeared as Fe content increased gradually and can be assigned to symmetrical and spin-forbidden d−d transitions of Fe^{3+} (Chmielarz *et al.*, 2007).

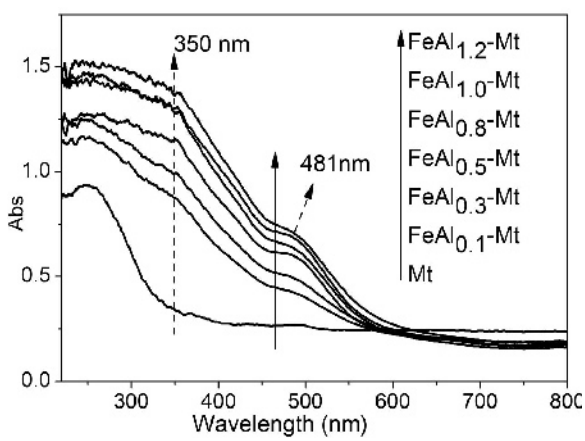

Figure 4. UV-vis diffuse reflectance spectra of montmorillonite and Fe/Al-Mt.

Catalytic activity of Fe/Al-Mt

Effect of synthesis method and Fe/Al ratio. A comparative study of effects of the synthesis method and the Fe/Al molar ratio on the photo-Fenton catalytic performance of the intercalated samples was conducted under the same experimental conditions. The degradation efficiency order was as follows: $0.5^a > 1.0 > 1.2^a > 0.8^a > 0.8 > 0.5 > 1.2 > 1.0^a > 0.3 > 0.2^a > 0.1$ (the number represented the Fe/Al molar ratio used in the

https://doi.org/10.1346/CCMN.2011.0590504 Published online by Cambridge University Press

preparation of catalyst; Figure 5). The best result in terms of degradation efficiency was $FeAl_{0.5}$-Mt[a] at 98.68%. The results for the next four samples ($FeAl_{1.0}$-Mt, $FeAl_{1.2}$-Mt, $FeAl_{0.8}$-Mt[a], and $FeAl_{0.8}$-Mt) were between 96.43% and ~95.47%, showing that the difference in degradation efficiency was not significant. The impact of aging temperature on the photocatalytic performance of the catalyst with the same Fe/Al ratio was notable. As the temperature increased from 30 to 60ºC, the degradation efficiency of the samples prepared at Fe/Al ratios of 0.5 and 1.2 was increased by 3.9% and 3.3%, respectively; at an Fe/Al ratio of 0.8, almost no change in the efficiency occurred, while for a ratio of 1.0, the efficiency decreased by 3.3%.

To select a catalyst for further study of the catalytic behavior of Fe/Al-Mt, three essential factors were considered: crystal structure (large basal spacing and large specific surface area), photocatalytic performance (efficiency at dye degradation), and practical issues (samples that are synthesized readily at room temperature were preferred). Based on characterization, analysis, and photocatalytic experiments, $FeAl_{0.8}$-Mt was chosen for further investigation.

Decoloration of X-GN by different reaction processes. Degradation experiments were carried out under different conditions to assess the effectiveness of the Fe/Al-Mt catalyst in photo-Fenton degradation of X-GN. The degradation efficiency was only 4.54% for the experiment in the presence of H_2O_2 and visible light (Figure 6), proving that the amount of hydroxyl radical generated under visible-light irradiation is rather small. Reaction in the presence of catalysts and visible light led to ~7.35% decoloration; a similar result was observed in previous work done on Fe-pillared clay (Chen *et al*., 2009). In a homogeneous Fe^{3+} solution and visible-light system, only a small amount of Malachite Green was photodegraded (Wu *et al*., 1999), suggesting that degradation of X-GN due to adsorption of the catalyst and oxidation of hydroxyl radicals generated by reaction of Fe with water under visible-light irradiation was quite limited. The Fenton process, conducted in the presence of a catalyst and H_2O_2 in the dark, showed a notable change in terms of decoloration of X-GN and achieved a degradation efficiency of 45.46% after 140 min. As visible light was applied to the Fenton reaction, the degradation efficiency improved to 95.47%. The photo-Fenton catalytic activity of the intercalated clay was, therefore, attributed to its potential to utilize visible light. The band gap of montmorillonite and $FeAl_{0.8}$-Mt was determined by means of the Kubelka-Munk formalism (equation 1) using UV-Vis spectra. The band gap of montmorillonite was 3.5 eV, while the

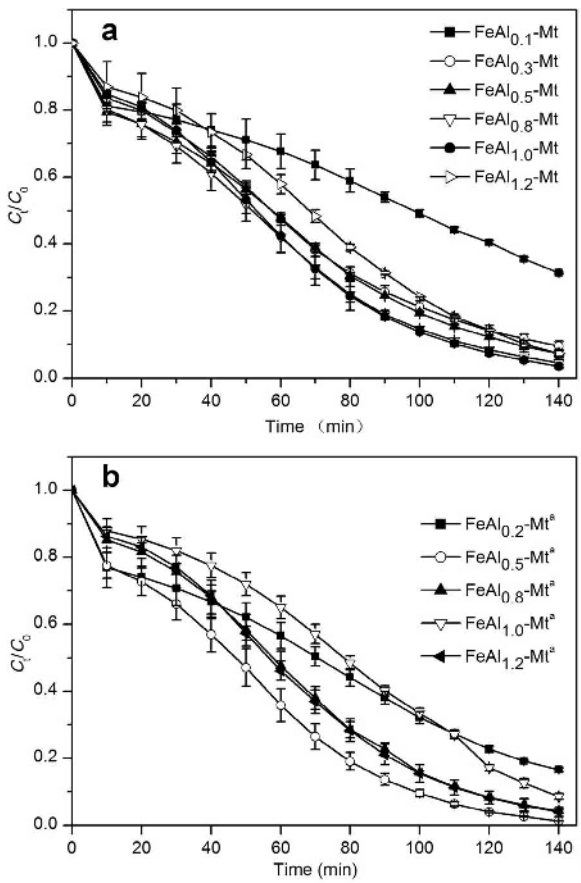

Figure 5. Comparative degradation profiles of X-GN in the presence of (a) Fe/Al-Mt and (b) FeAl-Mt[a]. $[X\text{-}GN]_0$ = 100 mg L^{-1}, pH = 3.0, FeAl-Mt/FeAl-Mt[a] = 0.4 g L^{-1}, T = 30ºC, $[H_2O_2]_0$ = 3.92 mmol L^{-1}. Error bars denote 95% confidence intervals.

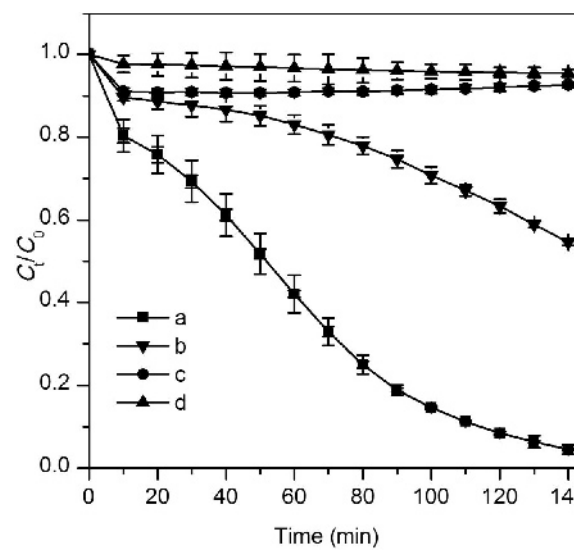

Figure 6. Decoloration of X-GN through different processes: (a) FeAl-Mt/H_2O_2/visible light, (b) FeAl-Mt/H_2O_2, (c) FeAl-Mt/visible light, and (d) H_2O_2/visible light. $[X\text{-}GN]_0$ = 100 mg L^{-1}, pH = 3.0, $FeAl_{0.8}$-Mt = 0.4 g L^{-1}, T = 30ºC, $[H_2O_2]_0$ = 3.92 mmol L^{-1}. Error bars denote 95% confidence intervals.

https://doi.org/10.1346/CCMN.2011.0590504 Published online by Cambridge University Press

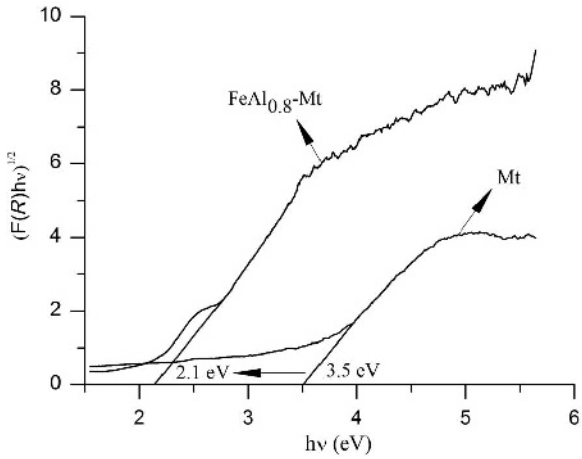

Figure 7. Determination of the (Kubelka-Munk) band gap between montmorillonite and $FeAl_{0.8}$-Mt.

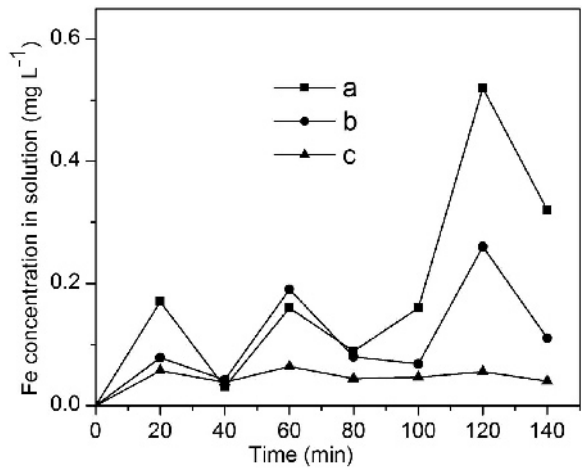

Figure 8. Fe leached from catalysts into solution under different processes: (a) FeAl-Mt/H_2O_2/visible light, (b) FeAl-Mt/H_2O_2, and (c) FeAl-Mt/visible light.

value was 2.1 eV for $FeAl_{0.8}$-Mt (Figure 7). The band gap shifted into the visible-light range meaning that the catalyst became more excitable under visible-light irradiation and thus could increase the degradation efficiency (Herrera *et al.*, 2003) (equations 2–4).

$$F(R) = \frac{(1-R)^2}{2R} \quad (1)$$

where R is reflectance (%).

$$\text{X-GN} + Fe^{3+} + h\nu \rightarrow \text{X-GN}^{+} + Fe^{2+} \quad (2)$$

$$Fe^{2+} + H_2O_2 \rightarrow Fe^{3+} + OH\cdot \quad (3)$$

$$\text{X-GN}^{+} + OH\cdot \rightarrow \text{degradated products} \quad (4)$$

The concentration of total Fe in solution measured by atomic absorption spectroscopy (AAS) revealed that the Fe was leached from the catalyst quite slowly ($<4.4 \times 10^{-3}$ mg L^{-1} min^{-1}) (Figure 8), indicating that the intercalated clay was very stable during the oxidation process. The maximum Fe concentrations in the photo-Fenton and Fenton processes were found to be 0.52 mg/L and 0.26 mg/L, respectively, for t = 120 min, which then decreased to 0.32 and 0.11 mg/L, respectively, due to adsorption of the catalyst, corresponding to 1.4% and 0.48% of the Fe loading of 0.08 g Fe/Al-Mt, respectively. The low Fe-leaching concentration suggests that the degradation of X-GN is mainly attributed to the heterogeneous photo-Fenton process. During the reaction, desorption and adsorption of Fe may take place at the same time, indicated by the increase and decrease in Fe concentration in the reaction time. Because the pH and intermediates that affected the desorption-adsorption process changed as the reaction proceeded, the Fe leaching became complex and did not simply increase gradually.

Effect of catalyst dosage

The degradation efficiency after 140 min was limited (95.47%) at low catalyst dosage (0.4 g L^{-1}) (Figure 9), due to the small adsorption quantity of the catalyst and lack of Fe species to act with OH· radicals. As the catalyst dosage increased to 0.5 g L^{-1}, almost complete removal of the dye removal could be achieved (99.92%) at 140 min. However, further increase in catalyst dosage led to a decrease in degradation rate, *i.e.* though nearly 50% degradation efficiency was obtained within 10 min using an added catalyst amount of 1.0 g L^{-1}, the final efficiency was <0.5 g L^{-1}. High density of clay tended to cause clay particles to agglomerate even under magnetic stirring, resulting in poor visibility in the solution and fewer active sites provided for decomposition of H_2O_2. The reduced rate of degradation with increased catalyst dosage may have arisen from less

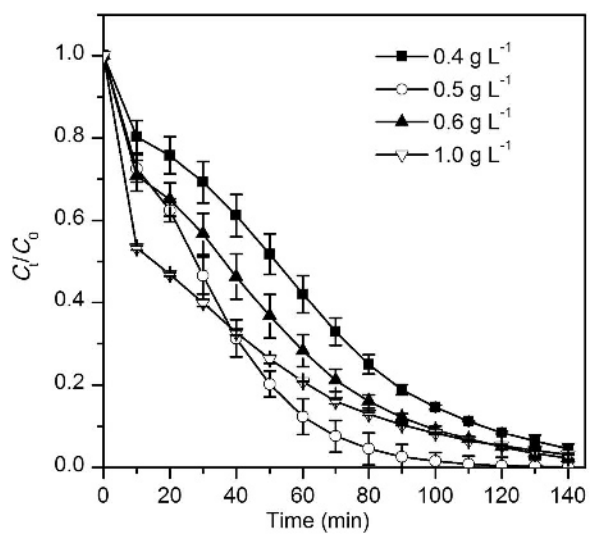

Figure 9. Effect of Fe/Al-Mt dosage on the degradation of X-GN. $[\text{X-GN}]_0$=100 mg L^{-1}, pH = 3.0, T = 30ºC, $[H_2O_2]_0$ = 3.92 mmol L^{-1}. Error bars denote 95% confidence intervals.

https://doi.org/10.1346/CCMN.2011.0590504 Published online by Cambridge University Press

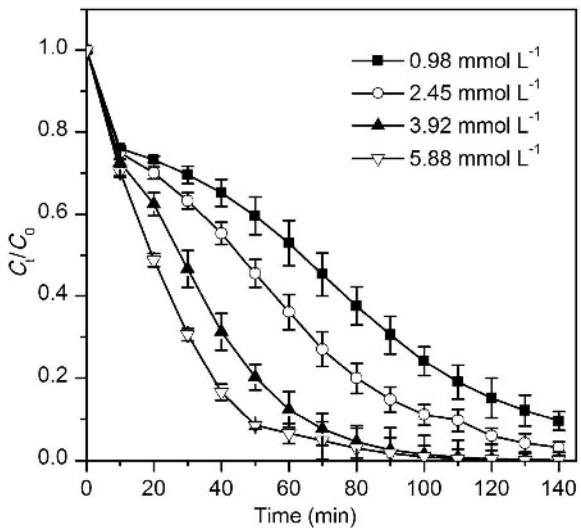

Figure 10. Influence of initial concentration of H_2O_2 on the degradation of X-GN. $[X\text{-}GN]_0$ = 100 mg L^{-1}, pH = 3.0, T = 30ºC, $FeAl_{0.8}$-Mt = 0.5 g L^{-1}. Error bars denote 95% confidence intervals.

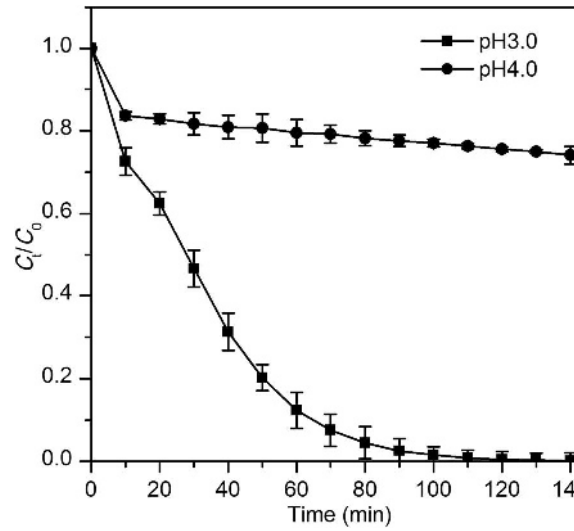

Figure 11. Effect of pH on the degradation of X-GN. $[X\text{-}GN]_0$ = 100 mg L^{-1}, $[H_2O_2]_0$ = 3.92 mmol L^{-1}, T = 30ºC, $FeAl_{0.8}$-Mt = 0.5 g L^{-1}. Error bars denote 95% confidence intervals.

oxidation (which may have competed with the photo-degradation of X-GN) of more intermediate products generated at the beginning of the photo-Fenton process.

Effect of initial concentration of H_2O_2

The effect of initial concentration of H_2O_2 was evaluated by varying its concentration between 0.98 and 5.88 mmol L^{-1} (Figure 10). The rate of degradation increased with increasing H_2O_2 dosage, because the quantity of OH· was increased, thus enhancing the rate of degradation.

Effect of pH

The effect of pH on the photo-Fenton reaction, using Fe/Al-Mt as an heterogeneous catalyst, was examined here to assess performance in milder (pH>3) conditions. Many attempts have been made to find a novel catalyst that can work at pH 7. Fenton oxidation may work over an expanded pH range using modified clays as heterogeneous catalysts (Sanabria *et al.*, 2009; Luo *et al.*, 2009; Kasiri *et al.*, 2008). In the present study, however, as pH was increased from 3.0 to 4.0, the degradation efficiency declined abruptly from 99.93% to 25.93% (Figure 11). As the amount of catalyst used in the experiment was small, the total adsorption equilibrium could be established at t = 10 min with prior stirring in the dark for 15 min. Degradation of X-GN for periods between 10 and 140 min depended mainly on the photo-Fenton reaction. The slow increase in degradation efficiency between 10 min and 140 min from 16.42% to 25.93% suggested that the amount of X-GN which degraded predominantly *via* photo-Fenton reaction was very small. Meanwhile, the pH may also influence the adsorption of X-GN. As the pH of the system increased, the number of negatively charged sites increased, which does not favor the adsorption of dye anions, due to electrostatic repulsion (Özcan and Özcan, 2004).

Investigation of the X-GN degradation pathway in photo-Fenton reaction

The UV-vis spectra of X-GN solution using 0.5 g L^{-1} catalyst dosage illustrated the transformation of X-GN during the photo-Fenton reaction under visible light (Figure 12). The change in spectra was similar to that from a previous study of degradation of X-GN (Chen *et*

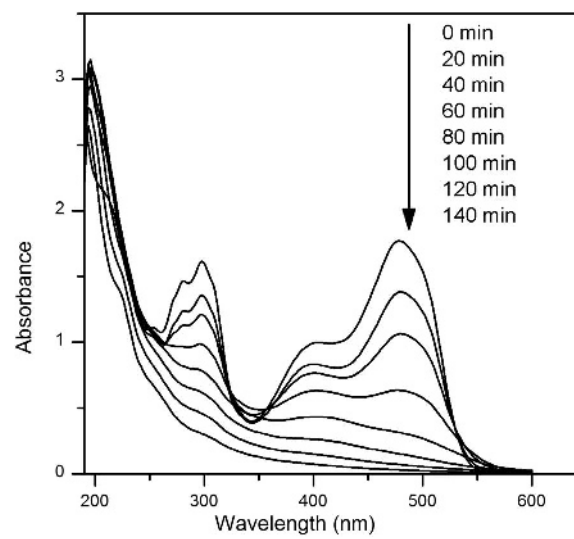

Figure 12. UV-vis spectra of X-GN solution during the photo-Fenton process in the presence of $FeAl_{0.8}$-Mt. $[X\text{-}GN]_0$ = 100 mg L^{-1}, pH = 3.0, $[H_2O_2]_0$ = 3.92 mmol L^{-1}, T = 30ºC, $FeAl_{0.8}$-Mt = 0.5 g L^{-1}.

https://doi.org/10.1346/CCMN.2011.0590504 Published online by Cambridge University Press

al., 2009). In the previous study, Fe-containing montmorillonite was used in which the photodecoloration of X-GN occurred firstly after breakage of −N=N− bonds (479 nm) and then after destruction of the long conjugated π* systems (298 nm) in the naphthalene ring. To understand intermediate products better, a liquid chromatography-mass spectrometry/mass spectrometry (LC-MS/MS) method was applied to identify the possible degradation products. Eight species of intermediate products were identified and reported with retention times on HPLC as well as the main fragments of the MS/MS spectra (Table 3).

Based on UV-vis spectra and information about intermediates derived from LC-MS/MS, a degradation pathway can be proposed (Figure 13). The results reveal that the attack of OH· radicals occurred not only at the −N=N− bond but also on the benzene and naphthalene rings, at different positions, due to the non-selective nature of OH·. The reaction seems to have been initiated by OH· radical attacks on the azo bond and NH−C,

Table 3. Intermediate products of X-GN identified using LC-MS/MS during the photo-Fenton process.

No.	Structure	Retention time (min)	Molecular weight	Main fragments (m/z) in MS/MS (relative abundance)
I1	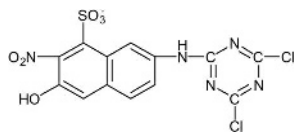	22.9	431	170 (50), 281 (34), 332 (26) 359 (41), 371 (23), 386 (22), 387 (100), 388 (35), 389 (42), 413 (33), 431 (48)
I2	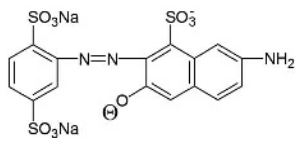	25.5	545	481 (100), 281(0.5), 331(0.4), 170(0.25), 361(0.3), 461(0.3), 485(0.3), 500(0.3), 525(0.3), 526(0.4)
I3	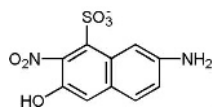	27.3	283	283 (100)
I4	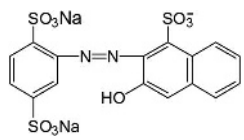	27.8	531	170 (22), 219 (17), 269 (39), 281 (100), 331(68), 282 (13), 381(28), 443 (20), 493 (11), 531 (26)
I5	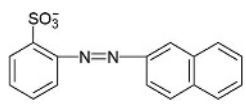	30.2	311	150 (60), 151(4), 171(3),184 (37), 185 (20), 309 (100), 247 (4), 311 (19)
I6	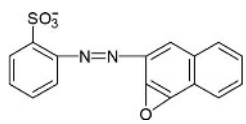	32.5	325	171 (6), 184 (86), 185 (22), 325 (100)
I7	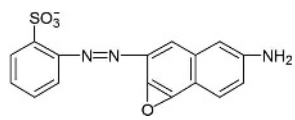	34.9	340	171 (5), 184 (100), 184 (21), 186 (7), 196 (5), 198 (51), 275 (5), 339 (76)
I8	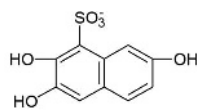	39	256	171 (28), 211 (17), 213 (11), 237 (52), 239 (13), 252 (13), 252 (12), 253 (100), 254 (11), 256 (68)

https://doi.org/10.1346/CCMN.2011.0590504 Published online by Cambridge University Press

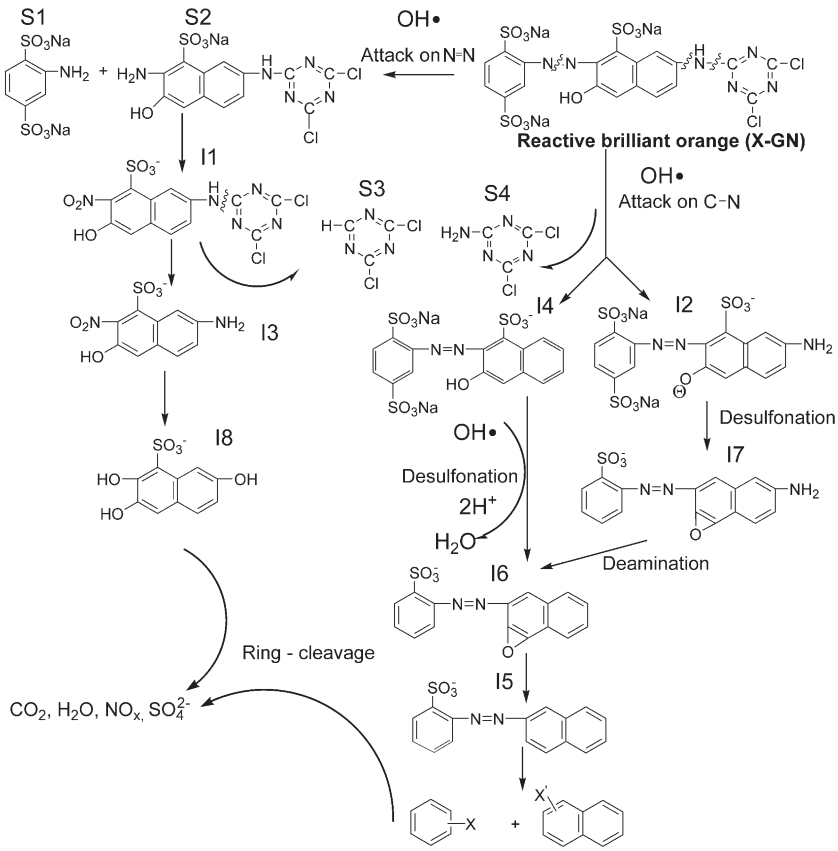

Figure 13. Proposed degradation pathway of X-GN by photo-Fenton reaction under visible light.

leading to the formation of several kinds of degradation products that can be classified into two major groups, one retaining the azo bonding and the other not. The hydroxyl radical attack on the azo bond and on the NH–C bond may give rise to the formation of compounds S1, S2, S3, and S4. These compounds were undetectable using the LC-MS/MS method, possibly because they are transient in the reaction. Oxidation, desulfonation, deamination, and hydroxylation reactions occurred, followed by breaking of the azo and NH–C bonds, leading to the formation of I1, I3, I5, I6, I7, and I8 (where I denotes intermediate products identified and S denotes putative intermediate products). In the cases of compounds I6 and I7, OH· radicals probably attacked the hydroxyl group contacts to the naphthalene ring and caused the loss of hydrogen. Finally, aromatic rings were destroyed, confirmed by the decrease in absorbance at ~298 nm.

CONCLUSIONS

Hydroxy Fe/Al intercalated montmorillonite was synthesized and applied as an heterogeneous photo-Fenton catalyst. The XRD results showed that the montmorillonite interlayer can be intercalated by the hydroxy Fe/Al species. A larger surface area was obtained after the intercalating process compared to the unmodified clay, which is beneficial for enhancing the adsorption quantity of the catalyst and facilitating the photocatalytic performance. Photocatalytic experiments were carried out under visible light: 99.92% degradation efficiency of X-GN was achieved under the following optimal conditions: $[X\text{-}GN]_0$ = 100 mg L^{-1}; $[FeAl_{0.8}\text{-}Mt]$ = 0.5 g L^{-1}; $[H_2O_2]_0$ = 3.92 mmol L^{-1}; pH = 3.0; and T = 30ºC. The present study demonstrated that Fe/Al-Mt is of practical use in the photo-Fenton degradation of X-GN, assisted by visible light.

ACKNOWLEDGMENTS

The present work was supported financially by the Program for National Natural Science Foundation of China (Grants No. 41073058, 40973075, 40730741); Research Fund for the Doctoral Program of Higher Education of China (No. 20100172110028); New Century Excellent Talents Program, Ministry of Education, China (Grant No. NCET-06-0747); Science and Technology Plan of Guangdong Province, China (Grants No. 2006B36601004, 2008B30302036, 2009B050900005); Natural Science Foundation of Guangdong Province, China (Grants No. 06025666, 9351064101000001); and the Fundamental Research Funds for the Central Universities, SCUT

https://doi.org/10.1346/CCMN.2011.0590504 Published online by Cambridge University Press

(Grants No. 2009ZZ0048, 2009ZZ0073, 2009ZM0202). The authors are grateful to the Analytical and Testing Center of South China University of Technology.

REFERENCES

Ali, I.O., Ali, A.M., Shabaan, S.M., and El-Nasser, K.S. (2009) Isomorphous substitution of Fe in the framework of aluminosilicate MFI by hydrothermal synthesis and their evaluation in p-nitrophenol degradation. *Journal of Photochemistry and Photobiology A: Chemistry*, **204**, 25–31.

Aouad, A., Anastácio, A.S., Bergaya, F., and Stucki, J.W. (2010) A Mössbauer spectroscopic study of aluminum- and iron-pillared clay minerals. *Clays and Clay* Minerals, **58**, 164–173.

Bachari, K., Millet, J.M.M., Bonville, P., Cherifi, O., and Figueras, F. (2007) Spectroscopic characterization of iron nanoparticles in Fe-mesoporous silicate catalysts. *Journal of Catalysis*, **249**, 52–58.

Barrault, J., Abdellaoui, M., Bouchoule, C., Majesté, A., Tatibouët, J.M., Louloudi, A., Papayannakos, N., and Gangas, N.H. (2000) Catalytic wet peroxide oxidation over mixed (Al-Fe) pillared clays. *Applied Catalysis B: Environmental*, **27**, 225–230.

Booij, E., Kloprogge, J.T., and vanVeen, J.A.R. (1996) Large pore REE/Al pillared bentonites: Preparation, structural aspects and catalytic properties. *Applied Clay Science*, **11**, 155–162.

Carriazo, J.G., Forero, M.M., Molina, R.A., and Moreno, S. (2010) Incorporation of titanium and titanium-iron species inside a smectite-type mineral for photocatalysis. *Applied Clay Science*, **50**, 401–408.

Carriazo, J.G., Molina, R., and Moreno, S. (2008) A study on Al and Al-Ce-Fe pillaring species and their catalytic potential as they are supported on a bentonite. *Applied Catalysis A: General*, **334**, 168–172.

Catrinescu, C., Teodosiu, C., Macoveanu, M., Miehe-Brendlé, J., and Dred, R.L. (2003) Catalytic wet peroxide oxidation of phenol over Fe-exchanged pillared beidellite. *Water Research*, **37**, 1154–1160.

Caudo, S., Centi, G., Genovese, C., and Perathoner, S. (2007) Copper- and iron-pillared clay catalysts for the WHPCO of model and real wastewater streams from olive oil milling production. *Applied Catalysis B: Environmental*, **70**, 437–446.

Chen, Q., Wu, P., Li, Y., Zhu, N., and Dang, Z. (2009) Heterogeneous photo-Fenton photodegradation of reactive brilliant orange X-GN over iron-pillared montmorillonite under visible irradiation. *Journal of Hazardous Materials*, **168**, 901–908.

Chmielarz, L., Kuśtrowski, P., Dziembaj, R., Cool, P., and Vansant, E.F. (2007) Selective catalytic reduction of NO with ammonia over porous clay heterostructures modified with copper and iron species. *Catalysis Today*, **119**, 181–186.

Cristofara, A.D. and Violante, A. (2001) Effect of hydroxy-aluminium species on the sorption and interlayering of albumin onto montmorillonite. *Applied Clay Science*, **19**, 59–67.

Dogan, M., Dogan, A.U., Yesilyurt, F.I., Alaygut, D., Buckner, I., and Wurster, D.E. (2007) Baseline studies of the Clay Minerals Society special clays: specific surface area by the Brunauer Emmett Teller (BET) method. *Clays and Clay Minerals*, **55**, 534–541.

Fejes, P., Kiricsi, I., Kovács, K., Lázár, K., Marsi, I., Oszkó, A., Rockenbauer, A., and Schay, Z. (2002) Incorporation of iron in sodalite structures and their transformation into other iron containing zeolites – synthesis of Fe-NaA (LTA). *Applied Catalysis A: General*, **223**, 147–160.

Guélou, E., Barrault, J., Fournier, J., and Tatibouët, J.-M. (2003) Active iron species in the catalytic wet peroxide oxidation of phenol over pillared clays containing iron. *Applied Catalysis A: General*, **44**, 1–8.

Herrera, F., Kiwiwi, J., Lopez, A., and Nadtochenko, V. (1999) Photochemical decoloration of Remazol Brilliant Blue and Uniblue A in the presence of Fe^{3+} and H_2O_2. *Environmental Science and Technology*, **33**, 3145–3151.

Jiang, J.Q., Cooper, C., and Ouki, S. (2002) Comparison of modified montmorillonite adsorbents – part I: Preparation, characterization and phenol adsorption. *Chemosphere*, **47**, 711–716.

Kasiri, M.B., Aleboyeh, H., and Aleboyeh, A. (2008) Degradation of acid blue 74 using Fe-ZSM5 zeolite as a heterogeneous photo-Fenton catalyst. *Applied Catalysis B: Environmental*, **84**, 9–15.

Kavitha, V. and Palanivelu, K. (2004) The role of ferrous ion in Fenton and photo-Fenton processes for the degradation of phenol. *Chemosphere*, **55**, 1235–1243.

Ladavos, A.K., Trikalitis, P.N., and Pomonis, P.J. (1996) Surface characteristics and catalytic activity of Al-pillared (AZA) and Fe-Al-pillared (FAZA) clays for isopropanol decomposition. *Journal of Molecular Catalysis A: Chemical*, **106**, 241–254.

Letaef, S., Blanca Casal, P.A., Martín-Luengo, M.A., and Ruiz-Hitzky, E. (2003) Fe-containing pillared clays as catalysts for phenol hydroxylation. *Applied Clay Science*, **22**, 263–277.

Luo, M.L., Bowden, D., and Brimblecombe, P. (2009) Catalytic property of Fe-Al pillared clay for Fenton oxidation of phenol by H_2O_2. *Applied Catalysis B: Environmental*, **85**, 201–206.

Madejová, J., Janek, M., Komadel, P., Herbert, H.-J., and Moog, H.C. (2002) FTIR analyses of water in MX-80 bentonite compacted from high salinity salt solution systems. *Applied Clay Science*, **20**, 255–271.

Molina, C.B., Casas, J.A., Zazo, J.A., and Rodríguez, J.J. (2006) A comparison of Al-Fe and Zr-Fe pillared clays for catalytic wet peroxide oxidation. *Chemical Engineering Journal*, **118**, 29–35.

Moreno, S., Kou, R.S., Molina, R., and Poncelet, G. (1999) Al-, Al,Zr-, and Zr-pillared montmorillonites and saponites: Preparation, characterization, and catalytic activity in heptane hydroconversion. *Journal of Catalysis*, **182**, 174–185.

Özcan, A.S. and Özcan, A. (2004) Adsorption of acid dyes from aqueous solutions onto acid-activated bentonite. *Journal of Colloid and Interface Science*, **276**, 39–46.

Ramirez, H., Silva, A.M.T., Vicente, M.A.V., Costa, C.A., and Madeira, L.M. (2011) Degradation of Acid Orange 7 using a saponite-based catalyst in wet hydrogen peroxide oxidation: Kinetic study with Fermi's equation. *Applied Catalysis B: Environmental*, **10**, 1–205.

Rao, G.R. and Mishra, B.G. (2005) A comparative UV-vis-diffuse reflectance study on the location and interaction of cerium ions in Al- and Zr-pillared montmorillonite clays. *Materials Chemistry and Physics*, **89**, 110–115.

Sanabria, N.R., Centeno, M.A., Molina, R., and Moreno, S. (2009) Pillared clays with Al-Fe and Al-Ce-Fe in concentrated medium: Synthesis and catalytic activity. *Applied Catalysis A: General*, **356**, 243–249.

Schwidder, M., Kumar, M.S., Klementiev, K., Pohl, M.M., Bruckner, A., and Grunert, W. (2005) Selective reduction of NO with Fe-ZSM-5 catalysts of low Fe content – I. Relations between active site structure and catalytic performance. *Journal of Catalysis*, **231**, 314–330.

Selvam, K., Swaminathan, K., and Chae, K.S. (2003) Decolourization of azo dyes and a dye industry effluent by

https://doi.org/10.1346/CCMN.2011.0590504 Published online by Cambridge University Press

a white rot fungus thelephora sp. *Bioresource Technology*, **88**, 115–119.

van der Zee, F.P. and Villaverde, S. (2005) Combined anaerobic-aerobic treatment of azo dyes – A short review of bioreactor studies. *Water Research*, **39**, 1425–1440.

Wu, K.Q, Xie, Y.D., Zhao, J.C., and Hidaka, H.(1999) Photo-Fenton degradation of a dye under visible light irradiation. *Journal of Molecular Catalysis A: Chemical*, **144**, 77–84.

Zhu, R.L., Wang, T., Ge, F., Chen, W.X., and You, Z.M. (2009) Intercalation of both CTMAB and Al_{13} into montmorillonite. *Journal of Colloid and Interface Science*, **335**, 77–83.

Zuo, S., Huang, Q., Li, J., and Zhou, R. (2009) Promoting effect of Ce added to metal oxide supported on Al pillared clays for deep benzene oxidation. *Applied Catalysis B: Environmental*, **91**, 204–209.

(*Received 11 September 2010; revised 22 September 2011; Ms. 493; A.E. H. Dong*)

https://doi.org/10.1346/CCMN.2011.0590504 Published online by Cambridge University Press